Chapter 4

4.1 Introduction

In this chapter, we have studied the structural and photoluminescence properties of HfO_2 and Sm doped HfO_2 nanoparticles synthesized by a Pechini type sol-gel technique. HfO_2 nanoparticles showing monoclinic phase transforms to the high temperature cubic phase upon doping Sm upto 12 at% followed by a mixed phase of monoclinic and cubic at intermediate concentration (5-11 at%) of Sm. Photoluminescence studies of HfO_2 demonstrate different strong emission bands in the visible region after exciting with UV light. Under excitation with visible light, the characteristic emissions of Sm^{3+} ion appear producing near green and red color light. A detailed phase transformation and photoluminescence behavior in Sm doped HfO_2 have been discussed.

4.2 Results and Discussion

4.2.1 Structure and Phase Transformation

X-ray diffraction (XRD) patterns of $Hf_{1-x}Sm_xO_2$ (x = 0-0.12) powders calcined at 900 ^oC in air are depicted in **figure 4.1(a)**.The XRD patterns show well distinguished, sharp diffraction peaks indicating crystalline nature of the particles. At x = 0, the observed diffraction peaks such as (011), (110), ($\bar{1}$11), (111), (020), (200), (021), ($\bar{2}$11) and (112) are indexed as the monoclinic phase of HfO_2 with space group, $P2_1/c$ (JCPDS card no. 78-0049). No secondary phase has been detected in the powders. While at x = 0.01, the diffraction peaks match well with the monoclinic phase, at $x \geq 0.05$, along with the diffraction peaks of the monoclinic phase, a weak peak at ~30.20^o is appeared which corresponds to (111), the most intense peak of the cubic phase (JCPDS card no. 53-0560).

Further increase in Sm concentration, the intensity of (111) increases. At $0.09 \leq x \leq 0.11$, although the diffraction peaks corresponding to both monoclinic and cubic phase are present, the cubic phase fraction increases at the expense of monoclinic one. At x = 0.12, it is evident that all diffraction peaks such as (111), (002), (022), (113) and (222) correspond to the pure cubic phase, space group, $Fm\bar{3}m$ of HfO_2. Absence of any impurity phase confirms that Sm^{3+} ions substitute Hf^{4+} ions in both monoclinic and cubic lattice. We, for the first time, demonstrate that the incorporation of Sm^{3+} ions into HfO_2 lattice stabilize the high temperature cubic phase of HfO_2 at room temperature. The phase transformation from monoclinic to cubic one with an increase in Sm concentration is accompanied with gradual change in phase fraction of monoclinic to cubic. We have estimated the phase fraction by taking the integral peak area ratio of (111) of cubic to (111) or ($\bar{1}$11) of monoclinic phase (**figure 4.1 (b)**). It is observed that the peak integral area ratio i.e. $A_{CP(111)}/A_{MP(111)}$ or $A_{MP(\bar{1}11)}$ increases with increase in Sm concentration. While a mixed phase of monoclinic and cubic exists at an intermediate Sm concentration (x = 0.05-0.11), the pure cubic phase of HfO_2 is observed at x = 0.12. The cubic phase of HfO_2 obtained after calcining at 900 ^oC, could be stabilized at room temperature by doping Sm upto 12 at%.

Further, the structural refinements are carried out using the Le-Bail profile fitting of FULLPROF program with pseudo-Voigt function. Typical observed and simulated XRD patterns for x = 0 and 0.12 using $P2_1/c$ and $Fm\bar{3}m$ are shown in **figure 4.2**. The observed pattern, simulated data after fitting and the difference pattern between observed and simulated data are shown as dots, continuous line and as bottom line, respectively. The tick marks above the difference plot show the positions of the Bragg peak. All the peaks corresponding to $P2_1/c$ and $Fm\bar{3}m$ are matched with observed peak positions.

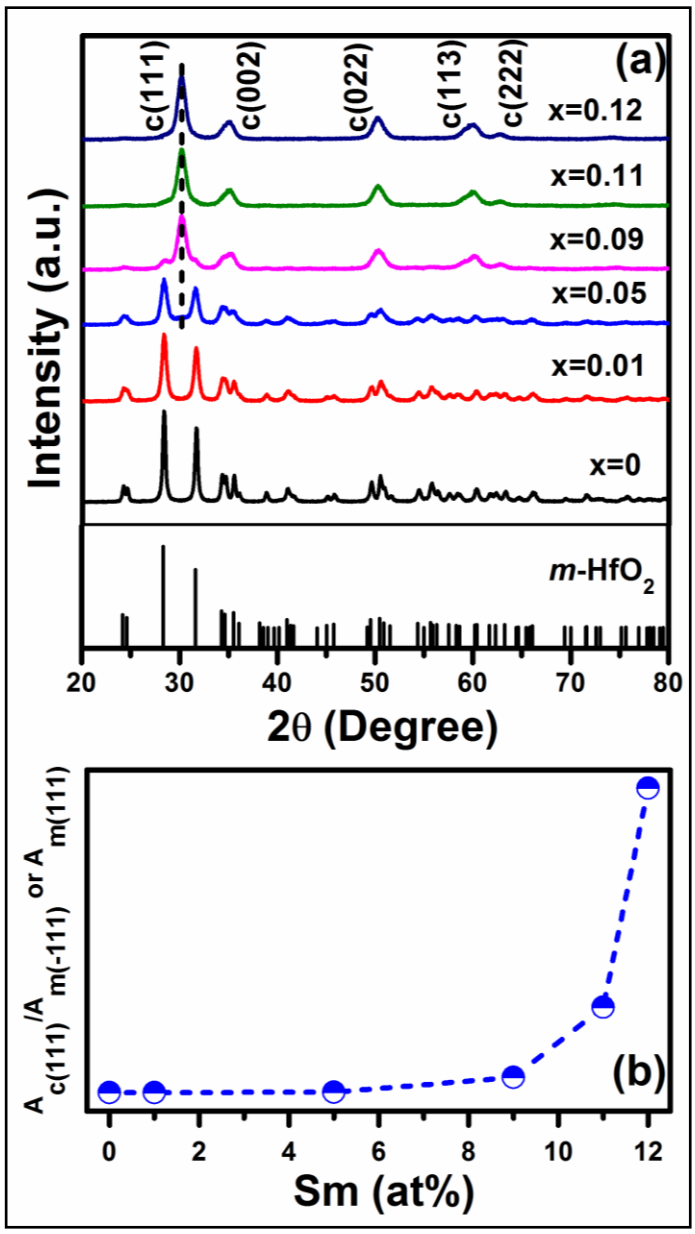

Figure 4.1 (a) *X-ray diffraction patterns of* $Hf_{1-x}Sm_xO_2$ *(0 ≤x ≤0.12) powders calcined at 900 °C and* ***(b)*** *integral peak area ratio of (111) of cubic phase to (T11) or (111) of monoclinic phase as a function of Sm concentration.*

The volume and cell parameters derived from the refinements are tabulated in **Table 4.1**.While lattice parameters of the monoclinic phase does not show any significant change compared to the standard value, in the cubic phase, '*a*' increases from 5.095 to 5.134 Å.

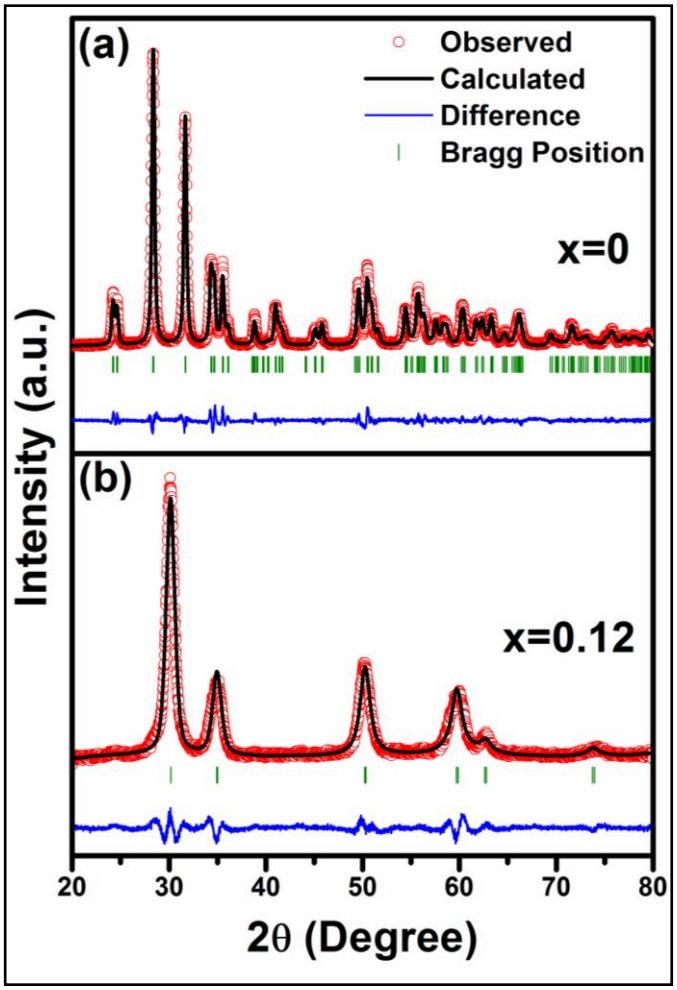

Figure 4.2 *Le-Bail profile fitting of $Hf_{1-x}Sm_xO_2$* ***(a)*** *x = 0 with $P2_1/c$ and* ***(b)*** *x = 0.12 with $Fm\bar{3}m$ space groups.*

JCPDS card no./Sample	Structure	Space group	Cell parameters			
			a (Å)	b (Å)	c (Å)	Volume (Å^3)
78-0049	Monoclinic	$P2_1/c$	5.117	5.175	5.291	138.32
53-0560	Cubic	$Fm\bar{3}m$	5.095	5.095	5.095	132.26
$Hf_{1-x}Sm_xO_2$ (x=0)	Monoclinic	$P2_1/c$	5.117	5.176	5.290	138.30
$Hf_{1-x}Sm_xO_2$ (x=0.12)	Cubic	$Fm\bar{3}m$	5.134	5.134	5.134	135.22

Table 4.1 *Refined cell parameters and cell volume for $Hf_{1-x}Sm_xO_2$ (x = 0 and 0.12) compared with standard JCPDS data for monoclinic and cubic phase of HfO_2*

Consequently, the cell volume of cubic phase shows an increment of 2.3%. The considerable enhancement in cell volume is in agreement with the increase in the ionic radius of Sm^{3+} ion (1.079 Å) than that of Hf^{4+} (0.83 Å) one. Such observation in Sm doped HfO_2 further endorses the substitution of Sm^{3+} at Hf^{4+}sites in the lattice favoring the stabilization of the high temperature cubic phase of HfO_2 at room temperature. Because of significant difference in ionic radii i.e. ~0.25 Å, it is worth to examine strain in the lattice with an increase in Sm concentration. Therefore, we have examined the Williamson-Hall (W-H) plot using following expression where ε is the lattice strain and D is the crystallite size.[141]

$$\frac{\beta \mathrm{Cos}\,\theta}{\lambda} = \frac{\mathrm{k}}{\mathrm{D}} + \frac{4\varepsilon \mathrm{Sin}\,\theta}{\lambda} \qquad (1)$$

In this plot, $\beta\mathrm{Cos}\theta/\lambda$ is plotted as a function of $\mathrm{Sin}\theta/\lambda$ where θ is Bragg angle, λ is the wavelength of X-ray, k is constant related to shape of particle and β is full width at half maximum (FWHM in radians) taken after removing $K\alpha_2$ contribution and instrumental broadening effects. In case of pure particle size broadening, this plot is likely to be a straight line parallel to $4\mathrm{Sin}\theta/\lambda$ at x-axis, whereas it shows a non-zero slope in the presence of strain in the lattice.[142] The change in particle size and lattice strain as a function of Sm concentration is depicted in **figure 4.3**. It is observed that upto x = 0.09, XRD peak broadening is only due to the particle size. The particle size found to be ~35 nm at x = 0 reduces substantially to ~20 nm at x = 0.01. No significant change in particle size observed upto x = 0.09. At x > 0.09, while the lattice strain increases and is enhanced by two orders of magnitude at x = 0.12, particle size is reduces ~10 nm.

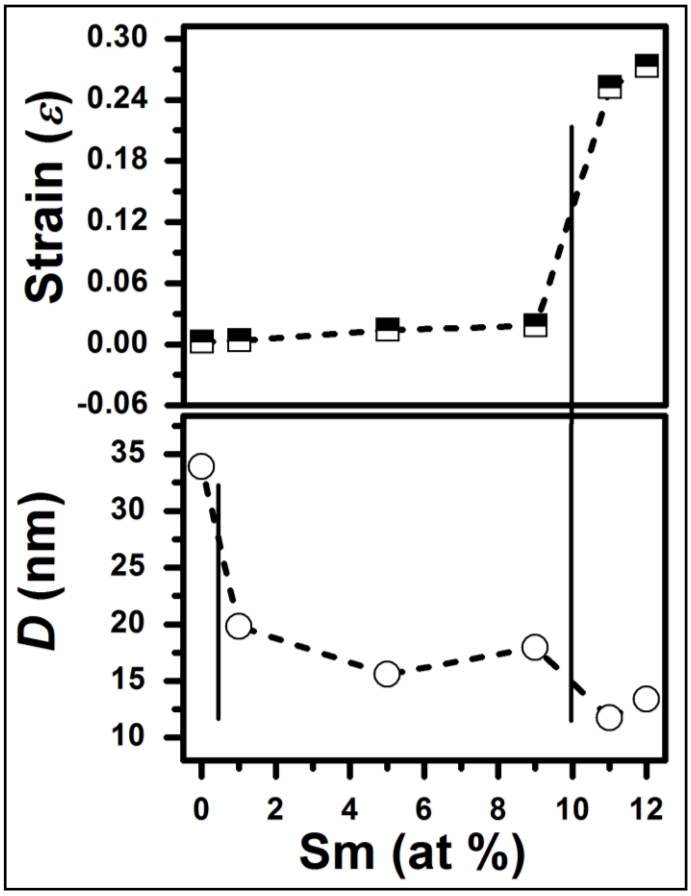

Figure 4.3 *Variation of crystallite size (D) and lattice strain (ε) in $Hf_{1-x}Sm_xO_2$ ($0 \leq x \leq 0.12$) obtained from Williamson-Hall plot.*

4.2.2 Microstructural Analysis

In order to further confirm the monoclinic and cubic phase, we have taken the selected area electron diffraction (SAED) pattern of $Hf_{1-x}Sm_xO_2$ (x = 0 and 0.12) as shown in **figure 4.4 (a) and (b)**. The well-defined diffraction rings in SAED are indexed as $(\bar{1}11)$, $(\bar{1}02)$, $(\bar{1}21)$ and $(\bar{2}13)$ of $P2_1/c$ and (111), (200), (220) and (311) of $Fm\bar{3}m$, respectively. The high resolution TEM images show different lattice planes in x=0 and 0.12 depicted in **figure 4.4 (c) and (d)**. The estimated interplanar spacing, as ~0.387 and 0.28 nm correspond to (011) and (111) of $P2_1/c$. The lattice planes with spacing of ~0.174 or ~0.206

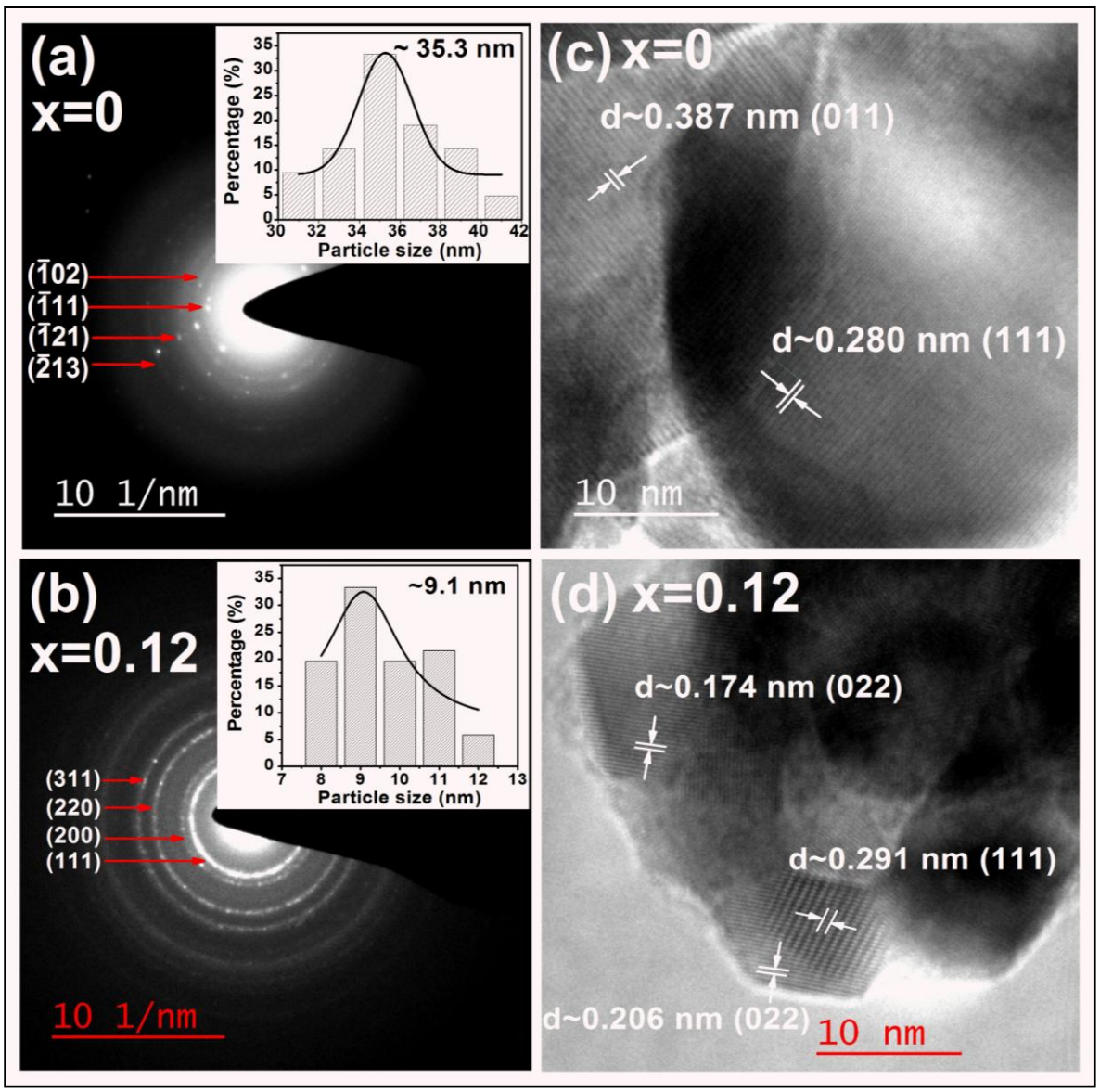

Figure 4.4 *SAED patterns of* ***(a)*** HfO_2 *and* ***(b)*** $Hf_{0.88}Sm_{0.12}O_2$ *and; High resolution TEM showing different lattice planes of* ***(c)*** HfO_2 *and* ***(d)*** $Hf_{0.88}Sm_{0.12}O_2$*. The particle size distribution histograms are shown as inset of* ***(a)*** *for* HfO_2 *and inset* ***(b)*** *for* $Hf_{0.88}Sm_{0.12}O_2$*.*

and ~0.291 nm are associated to (022) and (111) of $Fm\bar{3}m$. Transmission electron micrographs show that the particles are agglomerated and semi-spherical in shape (see **figure 3.6**). The particle size distribution histograms reveal that the average particle size is

found to be ~35 nm for x = 0 and ~9 nm for x = 0.12 (see insets of **figure 4.4 (a) and (b)**) which matches well with the average particle size calculated from W-H plot.

4.2.3 Mechanism for Monoclinic to Cubic Phase Transformation

Bulk HfO_2 possesses different polymorphs such as monoclinic, tetragonal and cubic phase. While monoclinic phase is stable at room temperature, HfO_2 undergoes a phase transition to the tetragonal and cubic phase at ~1700 and ~2600 ^oC, respectively. According to previously reported literature, the stabilization of the high temperature cubic phase of HfO_2 at room temperature can be achieved by incorporating dopants such as Mn, Ce, Lu, Dy and Y with different charge states.[54, 109, 111, 143, 144] In this context, Gao *et al.* synthesized Mn doped HfO_2 nanoparticles through a solid state reaction method and demonstrate the stabilization of the cubic phase within a narrow composition range of 20-30% of Mn.[109] It has been revealed that the monoclinic to cubic phase transformation involves the combined effect of size of Mn ion and charge states. Gálvez-Barboza *et al.* have achieved the cubic phase in 10 wt% Ce doped HfO_2 synthesized by a modified sol-gel technique.[143] Mendoza-Mendoza *et al.* prepare pure cubic HfO_2 nanoparticles by incorporating 10 mol% of Ce at lower temperature. A eutectic mixture of LiCl/KCl is employed as a molten flux to synthesize Ce doped HfO_2 nanoparticels as an alternate to conventional solid state route.[145] Matović *et al.* report the stabilization of the cubic phase of HfO_2 at room temperature after doping 20 mol% of yttrium.[111] We have recently shown that by incorporating Dy upto 11 at%, the monoclinic phase of HfO_2 transforms to the high temperature cubic phase which remains stable at room temperature. The stabilization of the cubic phase is ascribed to the formation of oxygen vacancies generated by the substitution of Dy^{3+} ions at Hf^{4+} ion site.[144] It is supported by the first

principle calculation which predicts that when a trivalent dopant cation substitutes Hf^{4+} ion, the deficiency of electrons in the host lattice occur and results in the formation of oxygen vacancies (V_o) due to charge compensation.[146, 147] The amount of oxygen vacancies vary with increase in trivalent dopant concentration. The incorporation of trivalent dopants in HfO_2 lattice lead to reduction in the formation energy to produce an oxygen vacancy. It is well known that in monoclinic HfO_2, the coordination number of Hf^{4+} cation is 7, whereas the coordination number in high symmetry cubic phase of HfO_2 is 8.[146] In the present case, when theSm^{3+} ions having a lower charge state and a larger ionic radius, replace Hf^{4+} ions, the oxygen vacancies are generated which prefer to reside near Hf atoms and leave 8-fold oxygen coordination to Sm^{3+} ions in the host lattice.WhenSm^{3+}ion concentrations are low, due to insufficient amount of oxygen vacancy, HfO_2exhibits the monoclinic phase and Hf is covalently bonded with O favoring 7-fold Hf coordination. With increase in Sm concentration, the energy needed to form an oxygen vacancy significantly decreases. As a result, a mixed phase of the monoclinic and cubic is observed for $0.05 \leq x \leq 0.11$. When a sufficient number of Sm^{3+} ion forming a 8-fold coordination with oxygen ion are present in the lattice, the high temperature cubic phase of HfO_2 becomes stable even at room temperature. At $x = 0.12$, there exists a nominal concentration of oxygen vacancies associated to Hf cation resulting in a 8-fold oxygen coordination to Sm^{3+} ions that surpass the 7-fold Hf coordination, thereby stabilizing the cubic phase at room temperature. Since RTFM behavior in Dy doped HfO_2 nanoparticles was quenched, we have not investigated the magnetic properties further.

4.2.4 Photoluminescence Properties

The monoclinic to cubic phase transformation driven by oxygen vacancies are further probed through its luminescence properties. The room temperature emission spectra of HfO_2 taken at the excitation wavelengths of 293 and 321 nm are shown in **figure 4.5 (a) and (b)**. Exciting HfO_2 under 293 nm, a broadband in the range of 360 to 550 nm showing a maximum at ~470 nm and two sharp emission peaks at 557 and ~613 nm are observed. The sharp peak located at 557 nm is attributed to 4-fold coordinated uncharged ($_{IV}V_o$) and single positively charged ($_{IV}V_o^+$) oxygen vacancies.[82, 147] The emission band at ~613 nm falling near red region could be due to $O(^1D) \rightarrow O(^3P)$ i.e. transition from singlet to triplet ground state of oxygen atom.[82, 148, 149] Due to the asymmetric shape of the broadband observed in the range of 360-550 nm, we have deconvoluted the spectrum into two distinct peaks named as peak 1 and 2located at 423 and 466 nm, respectively (see left inset of **figure 4.5 (a)**). While the former emission band (peak 1) is ascribed to 3-fold coordinated $_{III}V_o$ and the latter one (peak 2) could originate due to $_{III}V_o^+$.[82, 150, 151] Exciting HfO_2 with321 nm, except a significant increase in the intensity of peak at ~613 nm, no other peak is detected. Deconvoluted peaks such as peak 1 and 2 are found to be located at 440 and 479 nm indicating a red shift of ~15 nm. While peak 1 is quite suppressed under excitation wavelength of 293 nm, after exciting at 321 nm, the area under the peak is enhanced significantly.

Figure 4.6 (a), (b) and (c) depict the photoluminescence emission spectra of $Hf_{1-x}Sm_xO_2$ (x = 0,0.01, 0.05 and 0.12) excited at wavelength of 321, 410 and 465 nm, respectively. After exciting with 321 nm, HfO_2 shows emission peaks induced by oxygen vacancies related defects. In $Hf_{0.99}Sm_{0.01}O_2$, while the broadband is suppressed, emission

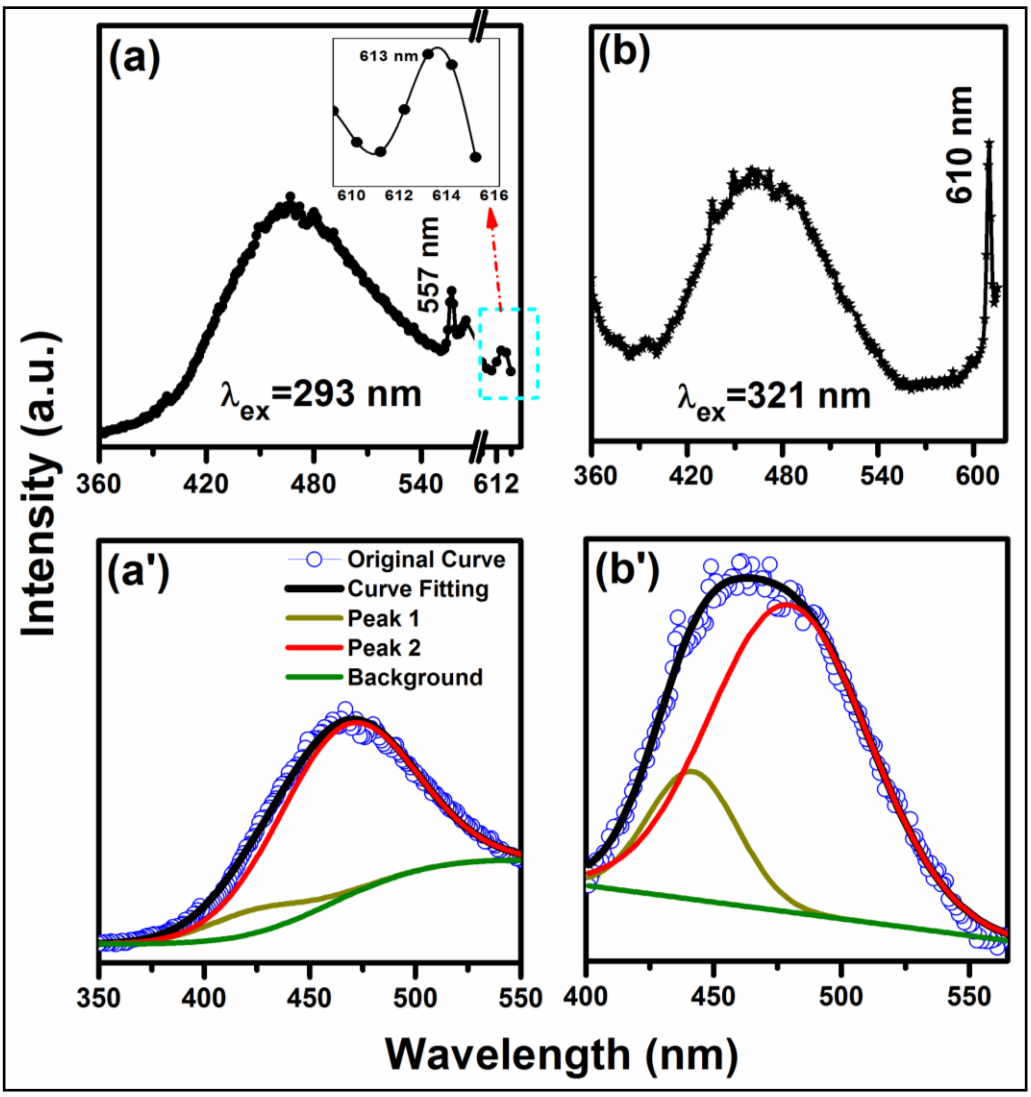

Figure 4.5 *Photoluminescence spectra of HfO_2 excited at* ***(a)*** *293 nm and* ***(b)*** *321 nm. The right inset of* ***(a)*** *shows emission peak at ~613 nm.****(a') and (b')****illustrate the deconvolution of broadband for 293 and 321 nm excitation wavelength, respectively.*

peak at ~613 nm of the host remain unchanged. With an increase in Sm concentration upto 12 at%, the intensity of peak at ~613 nm gradually decreases. Surprisingly, we do not observe any emission peak associated to Sm^{3+} activator ion when excited with either 293 nm or 321 nm. Exciting $HfO_2$with 410 nm, a significant sharp emission peak is observed at 557 nm (**figure 4.6 (b)**). It could be due to relaxation of electrons from ${}_{IV}V_o$ and ${}_{IV}V_o^{+}$ to

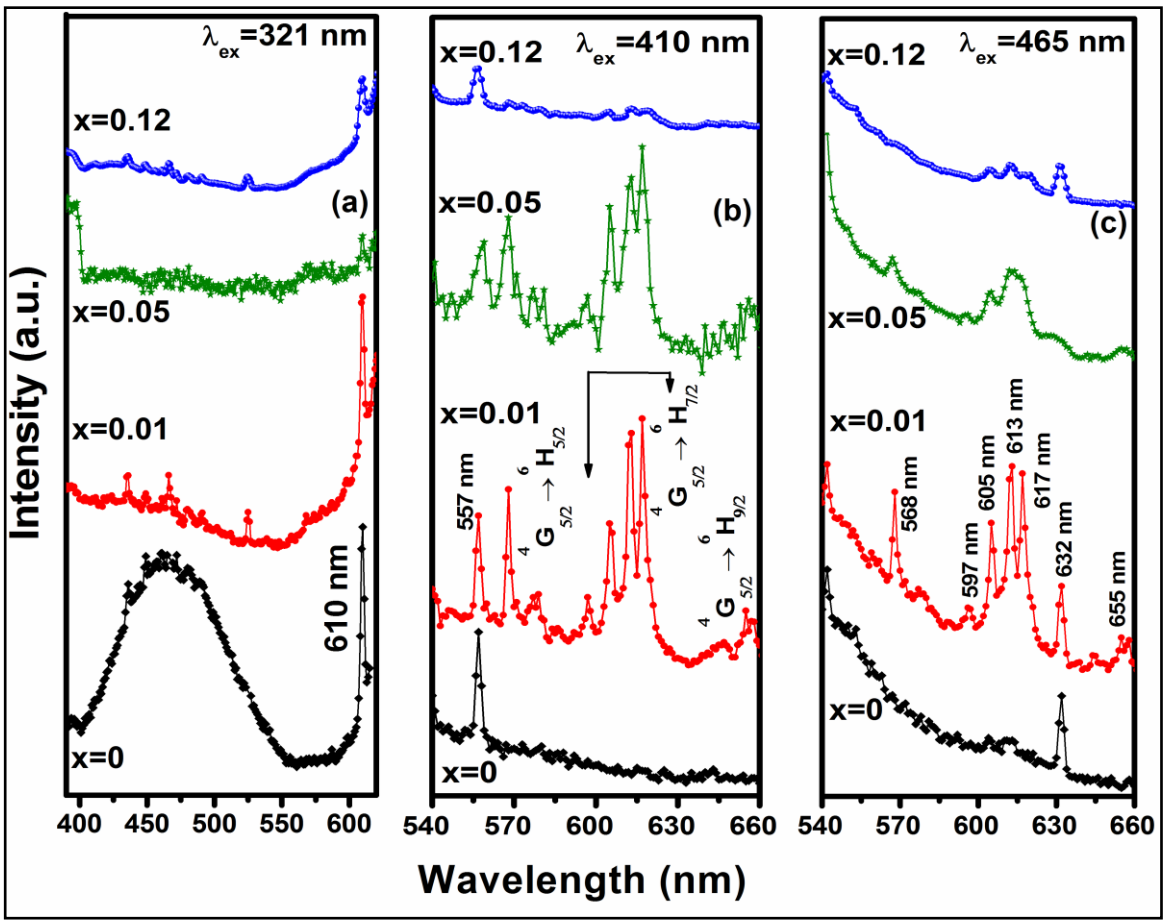

Figure 4.6 *Photoluminescence spectra of $Hf_{1-x}Sm_xO_2$ (x=0, 0.01, 0.05 and 0.12) excited at* ***(a)*** *321 nm,* ***(b)*** *410 nm and* ***(c)*** *465 nm.*

valence band of the host HfO_2.[82] After incorporating 1 at% of Sm, along with emission peak at 557 nm, the emission spectrum consists of several well resolved and distinct peaks at 568, 577, 597, 605, 613, 617 and 656 nm. These emission peaks emerge due to different *f-f* transition taking place within the energy level of Sm^{3+} activator ion. The set of peaks centered at 568 and 577 nm in green/yellow, 597-617 nm in near red and 656 nm in pure red region are attributed to the transition from $^4G_{5/2}$ to $^6H_{5/2}$, $^6H_{7/2}$ and $^6H_{9/2}$, respectively.[152, 153] Such a nature of the Sm^{3+} ion emission band is a characteristic of the Stark splitting induced because of the crystalline field of HfO_2. It is known that while

$^4G_{5/2} \rightarrow {}^6H_{5/2}$ is a magnetic dipole transition, $^4G_{5/2} \rightarrow {}^6H_{9/2}$ is an electric dipole transition which is hypersensitive to the crystal field environment. $^4G_{5/2} \rightarrow {}^6H_{7/2}$ exhibits a mix-up of electric and magnetic dipole transition components.[154] The low peak intensity corresponding to electric dipole transition than the magnetic one is an indication of the less asymmetric nature of the host HfO_2 lattice. The dominant nature of magnetic transition also demonstrates the presence of Sm^{3+} ion at a low symmetry site with an inversion symmetry in the host lattice.[154, 155] Further, the intensity of these emission peaks decreases with increasing Sm concentration to 5 at%. At Sm concentration of 12 at%, except the peak at 557 nm of the host, all other emission peaks are significantly suppressed. Under an excitation wavelength of 465 nm, in the emission spectrum of HfO_2, one can observe the host emission peak at 632 nm which is red shifted by ~20 nm (**figure 4.6 (c)**). In $Hf_{0.99}Sm_{0.01}O_2$, the spectrum exhibits all characteristic emission peaks of Sm^{3+} ion in the wavelength range of 540-660 nm. With increasing Sm concentration to 5 at%, all emission peaks become significantly broader and intensity decreases considerably. At x = 0.12, while emission peaks of Sm^{3+} ion are reduced drastically, the peak at 632 nm of the host remains present. The broadness of the peaks is attributed to difference in crystal field strength and to different local environment, in particular, the high symmetry of cubic phase in this case.[156] The drastic reduction in the intensity of the emission peaks could be due to the change in the local symmetry around Sm^{3+} ions. Besides the high symmetry, a higher Sm concentration leads to reduction in the mean distance between two Sm^{3+} ions. This results in the cross relaxation between themselves present at different sites in the lattice by non-radiative transition processes such as exchange interaction, radiation reabsorption or electric multipolar interaction.[157-159] Considering the fact that $Hf_{0.88}Sm_{0.12}O_2$ exhibits

the high symmetry cubic phase, the observed luminescence behavior is in agreement with reported literature which also supported by our XRD results.[54, 156, 157, 160] In this context, Rauwel *et al*. observe an emission peak at 3.1 eV (390-400 nm) in cubic phase HfO_2 stabilized using benzyl amine solvent.[51] However, this emission peak is not only absent in emission spectrum of $Hf_{0.88}Sm_{0.12}O_2$, but also in cubic phase stabilized using 7 at% of Lu in HfO_2:3.3% Eu and 10 mol% of Lu in HfO_2:1 mol% Eu do not show the emission peak at 3.1 eV.[156]

Since the host emission is observed at ~470 nm and characteristic emission of Sm^{3+} at 617 nm, we have taken the excitation spectra of HfO_2 and $Hf_{0.99}Sm_{0.01}O_2$ depicted in **Figure 4.7 (a)**. In HfO_2, it can be found that the excitation spectrum shows a broadband in the range of 250-350 nm with a maximum at ~293 nm. Another sharp peak is observed at 430 nm. While the former band is ascribed to the host absorption, the latter peak appears due to the defect states such as oxygen vacancies in HfO_2 lattice.[54, 144] However, for $Hf_{0.99}Sm_{0.01}O_2$, the broadband disappears completely and the peak at 430 nm remains present with reduced intensity. It is to be noted that no peak related to Sm^{3+} ion is observed. **Figure 4.7(b)** depicts the excitation spectra recorded by monitoring the characteristic emission peak at 617 nm corresponding to Sm^{3+} ion. In HfO_2, the spectrum exhibits peaks of low intensity in the wavelength range of 450-480 nm. This appears because of the host absorption to $_{III}V_o^+$ defect states. In addition, these peaks could correspond to the host emission observed at ~613 nm since it lies very near to the characteristic emission band of Sm^{3+} ion. However, for $Hf_{0.99}Sm_{0.01}O_2$, one can observe two prominent sharp peaks within the excitation spectrum. While the excitation peaks located within the wavelength range of 400-420 nm (maximum at 405 nm) originate due to

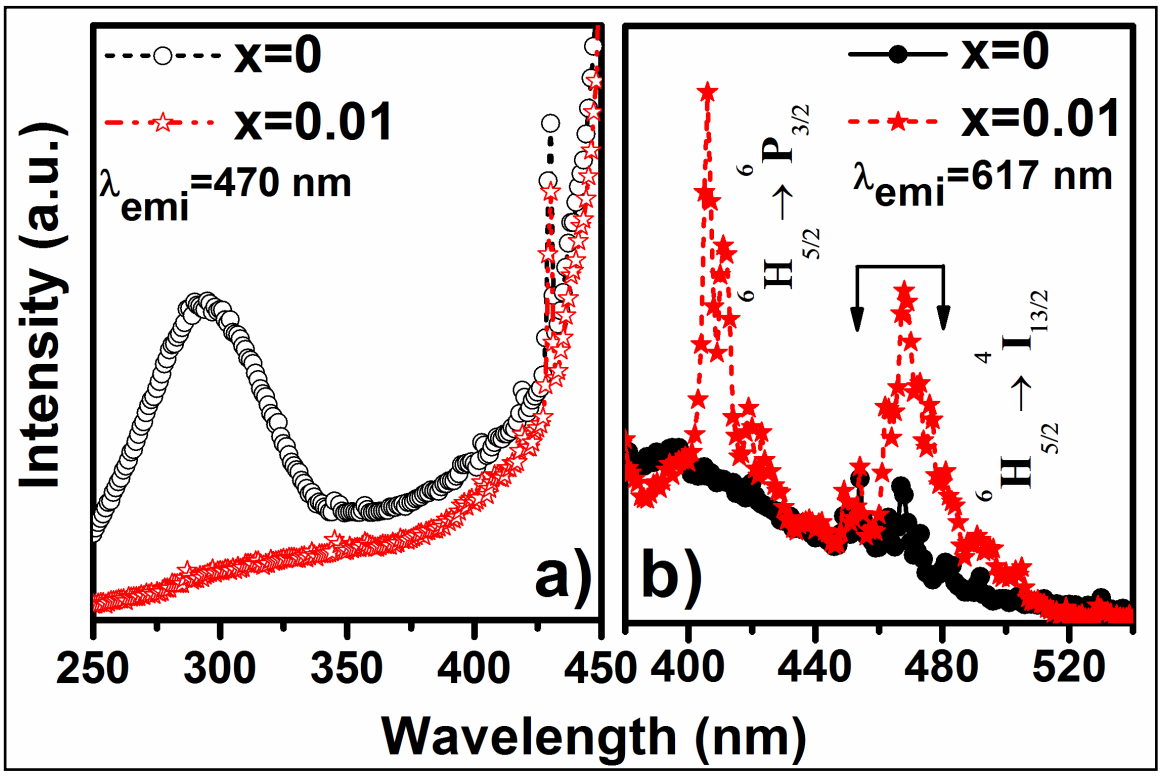

Figure 4.7 *Room temperature excitation spectra of HfO_2 and $Hf_{0.99}Sm_{0.01}O_2$ monitored at emission wavelength* ***(a)*** *470 nm and* ***(b)*** *617 nm.*

the transition $^6H_{5/2} \rightarrow {}^6P_{3/2}$, the peaks in the wavelength range of 460-490 nm (maximum at 468 nm) correspond to $^6H_{5/2} \rightarrow {}^4I_{13/2}$ transition of Sm^{3+} ion.[161] One may note that the excitation peaks within the wavelength range of 450-490 nm coexist for both HfO_2 and $Hf_{0.99}Sm_{0.01}O_2$. The similar peak positions in 460-490 nm range in the excitation spectra show that a few defect levels of HfO_2 takes part by transferring charge weakly to Sm^{3+}ion inducing their characteristic emissions. **Figure 4.8** depicts the two dimensional (x, y) CIE color space chromaticity diagram of $Hf_{1-x}Sm_xO_2$ (x = 0 and 0.01) under different excitation wavelengths. The CIE chromaticity coordinates of HfO_2 are found to be (0.18,0.26) and (0.26, 0.28) for λ_{ex} = 293 and 321 nm, respectively. For $Hf_{1-x}Sm_xO_2$ (x = 0.01), CIE

coordinated are (0.40, 0.50) and (0.28, 0.46) for λ_{ex} = 410 and 465 nm, respectively. Since the broadband in the range of 350-550 nm is dominating compared to emission peaks at557 and ~613 nm, the host HfO_2 emits a blue color light under an excitation wavelength of 293 nm. When excited with 321 nm, although the emission peak at 557 nm is disappeared, due to significant contribution from the emission peak at ~613 nm, the host HfO_2 produces a bluish cool white light. In $Hf_{1-x}Sm_xO_2$ (x = 0.01), we reveal near green and green-yellow emission from CIE diagram after exciting with 410 and 465 nm, respectively.

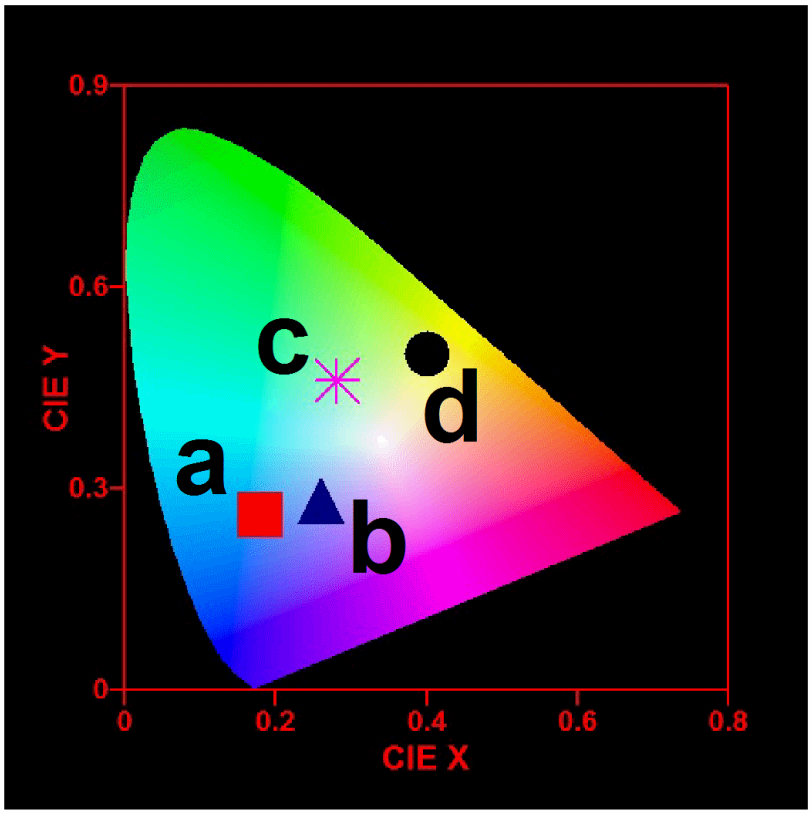

Figure 4.8 *The CIE color space chromaticity diagram (Point 'a' and 'b' correspond to HfO_2 for λ_{ex} = 293 and 321nm; 'c' and 'd' correspond to $Hf_{0.99}Sm_{0.01}O_2$ for λ_{ex} = 410 and 465 nm, respectively).*

4.2.5 Energy Band Diagram

In order to understand the detailed photoluminescence behavior of $Hf_{1-x}Sm_xO_2$, a schematic energy level diagram has been presented considering the different excitation and emission processes (**figure 4.9**). The various energy levels are specified as $^6P_{3/2}$, $^4I_{13/2}$, $^4G_{5/2}$, $^6H_{5/2}$, $^6H_{5/2}$ and $^6H_{5/2}$ corresponding to Sm^{3+} ion and $_{III}V_o$, $_{III}V_o^+$, $_{IV}V_o$, $_{IV}V_o^+$, O(^{1}D) and O(^{3}P) associated to the host HfO_2 lattice. Exciting with 293, 321, 410, 425 or 465 nm, electrons at valence band (VB) of HfO_2 are not excited to conduction band (CB) due to wide band gap of ~5.7 eV of HfO_2. The electrons can only be excited to the host charge transfer band (CTB) located below CB, after exciting with the highest energy i.e. lower excitation wavelength of 293 nm. The relaxation of excited electrons to VB through different defect levels show host related emissions as observed at 423, 466, 557 and ~613 nm from emission spectra of HfO_2 (**figure 4.5**). Exciting at 321 nm, we also observed similar emission peaks which are only host related emissions. In 1 at% Sm dopedHfO_2, no peak of Sm^{3+}ion is detected after exciting with either 293 or 321 nm which indicates the absence of charge transfer from the host CTB to Sm^{3+} activator ion. This is mainly because of the significant energy difference between the host CTB and emission level of Sm^{3+} ion. However, at higher excitation wavelengths of 410, 425 or 465 nm of visible range, along with one of the host emissions at ~557 or ~613 nm, characteristic emission peaks of Sm^{3+} ion are observed in the range of 568-580, 600-620 and 650-657 nm. Such emissions are only possible when there is a charge transfer from the defect levels of host to different energy levels of Sm^{3+} activator ion. Previously, we report that host CTB weakly sensitize sensitize the luminescence of Dy^{3+} ions producing bluish cool white emission (CIE coordinate: (0.27, 0.27) for 1 at% Dy).[144]

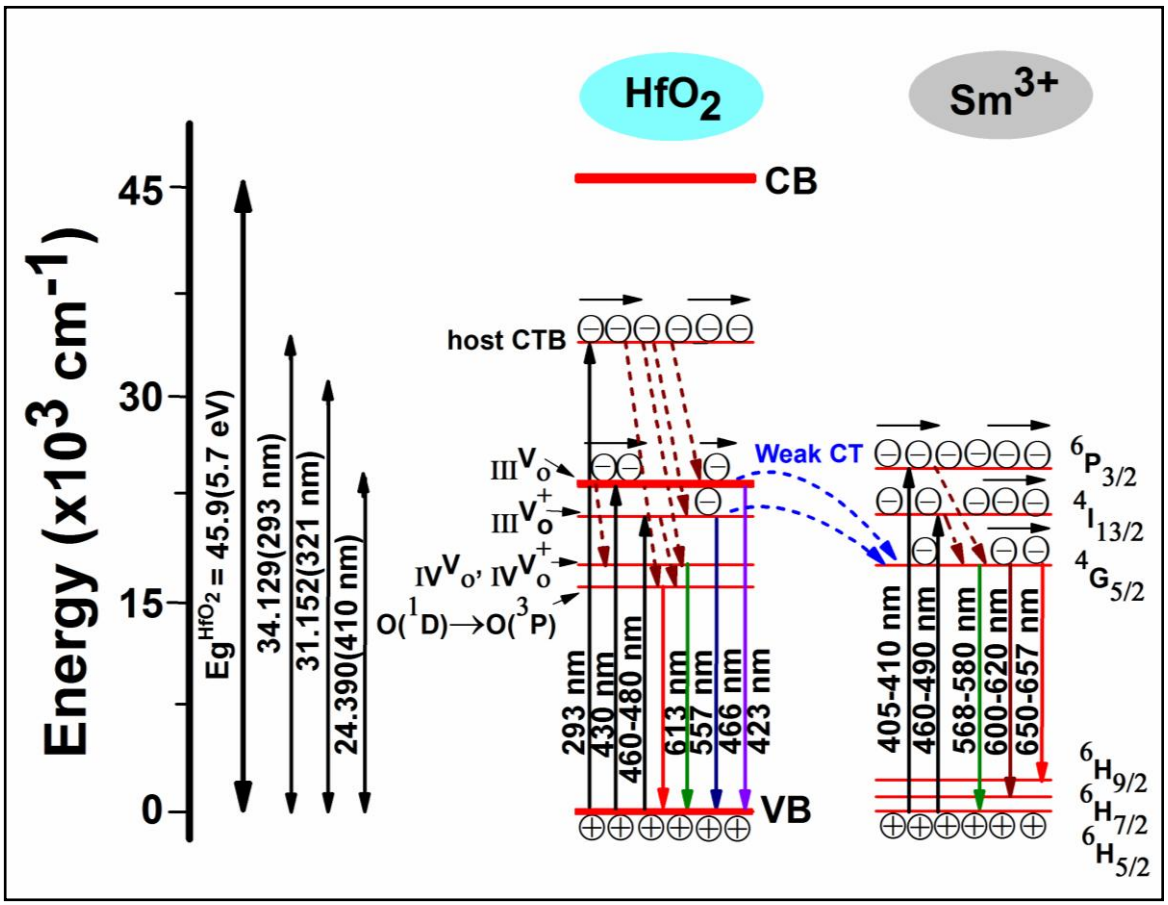

Figure 4.9 *A schematic energy band diagram showing the excitation and emission processes involved in* HfO_2 *and* $Hf_{0.99}Sm_{0.01}O_2$ *nanoparticles.*

Herein, under an excitation wavelength of 321 nm, without any rare earth ion, the host HfO_2 gives a similar CIE coordinate of (0.26, 0.28). While the host CTB do not transfer charge to Sm^{3+} ions exciting with UV light, the optically active oxygen related defect levels acting as sensitizers show weak charge transfer phenomenon when excited at energy comparable to the energy of defect levels of HfO_2. Therefore, one may note that in wide band gap oxides like HfO_2, by incorporating Sm^{3+} ion, it is possible to tune the light emissions producing a range of colors in visible region. These materials are thus important for optoelectronic device applications.

4.3 Conclusions

This chapter systematically investigated the structural and photoluminescence properties of HfO_2 and Sm doped HfO_2 nanoparticles with varying Sm concentration (1-12 at%). HfO_2 crystallized in monoclinic phase with an average particle size of ~35 nm. By incorporation of 5 at% of Sm into HfO_2 lattice, it could be possible to partly transform the monoclinic phase to cubic one. Above 5 at%, cubic phase fraction increased at the cost of monoclinic one and at x = 0.12, the cubic phase of HfO_2 was completely stabilized at room temperature. The phase transformation from the monoclinic to cubic phase was accompanied with dramatic enhancement of lattice strain and reduction in size analyzed from Williamson-Hall plot. A prospective role of Sm incorporation stabilizing the cubic phase in HfO_2 lattice has been examined considering the valency of Sm and difference in ionic radii of Sm^{3+} and Hf^{4+} ion. Selected area electron diffraction patterns and the lattice spacing estimated from high resolution TEM further confirmed the monoclinic, $P2_1/c$, and cubic, $Fm\bar{3}m$, phase in HfO_2 and $Hf_{0.88}Sm_{0.12}O_2$ nanoparticles, respectively. Being HfO_2 an outstanding host material, after Sm^{3+} ion incorporation, the photoluminescence studies

revealed an excellent emissions in near green and red region due to the charge transfer phenomenon occurring between the host and different energy levels of Sm^{3+} ion. Combining different excitation and emission processes, a schematic energy band diagram was proposed.